 CMES, vol.29, no.3, pp.163-173, 2008

Lattice Boltzmann Method Simulation of 3D Fluid Flow in Serpentine Channel

Shih-Kai Chien[1], Tzu-Hsiang Yen[1], Yue-Tzu Yang[1] and Chao-Kuang Chen[1,2]

Abstract: Conventional proton exchange membrane fuel cells (PEMFCs) have a straight gas flow serpentine channel, and hence the reactant gases are transferred to the catalyst layers as a result of diffusion alone. Since the diffusion process is inherently slow, the electrical performance of such PEMFCs is inevitably limited. In an attempt to improve the PEMFC performance, this study replaces the straight channel with containing different type of obstacles and conducts a series of lattice Boltzmann method simulations to investigate the flow field phenomena induced in a viscous liquid as it flows along the serpentine channel at Reynolds numbers ranging from Re=5∼25. The simulations consider three different channel configurations, namely an empty channel with planar walls, a channel containing 10 rectangular obstacles, and a channel containing 10 semi-circular obstacles. The numerical results show that the obstacles enhance the vertical velocity component of the flow and prompt the formation of recirculation regions immediately downstream of each obstacle. Both phenomena are beneficial in improving the performance of the PEMFC. Specifically, the velocity perturbations in the vertical direction increase the flow of the reactant gas into the gas diffusion layer and therefore improve the catalytic reaction performance, while the recirculation flow structures assist in the removal of the water byproduct from the cathode channel and therefore reduce the accumulation of water within the cathode channel.

Keyword: Lattice Boltzmann method, proton exchange membrane fuel cell (PEMC), serpentine channel

[1] Department of Mechanical Engineering, National Cheng Kung University, Tainan, Taiwan
[2] Corresponding author. Tel.: +886-6-2757575 ext. 62140; Fax: +886-6-2342081 E-mail: ckchen@mail.ncku.edu.tw

Nomenclature

AR	aspect ratio
c	lattice streaming speed f friction factor
c_s	speed of sound
C	shape factor
D_h	hydrodynamic diameter function for f_α
f_α	density distribution function
f_α^{eq}	equilibrium distribution
p	pressure
Re	Reynolds number
U	inlet velocity
$\vec{V}$	velocity vector

Greek symbols

τ_υ	relaxation time for f_α
ρ	density
υ	kinematic viscosity
δx	lattice spacing
δt	time step

Subscripts

m	mean

1 Introduction

Two dimentions (2D) incompressible viscous flow is a typical topic in the research of fluid flow [Nicolas and Bermudez (2004)] and is studied by the lattice Boltzmann method (LBM) in the recent years. The LBM has emerged as a powerful technique for the simulation of fluid flows and the modeling of general fluid physics [Chen and Doolen (1998)]. In the LBM approach, the flow

system is modeled by tracking the time-dependent evolution of individual particle distributions using a discretized single-particle phase space distribution function similar to that described by the traditional Boltzmann BGK (Bhatnagar-Gross-Krook) kinetic equation. The LBM technique is computationally straightforward, amenable to parallel processing and provides reliable results for a variety of complex fluid flow problems in the scientific and engineering domains [He, Chen, and Doolen (1998), Wolf-Gladrow (2000), Succi (2001)]. Chen, Chang, and Sun (2007) investigate the flow and heat transfer phenomena of the 2D channel flow by the LBM simulation. Qian, d'Humieres, and Lallemand (1992) applied D3Q15 and D3Q19 LBM models to solve the 3-D Navier-Stokes equation and in the following the more velocity set D3Q21 and D3Q25 model also recommended. By the coupled LBM and the discrete element method (DEM), Han, Feng, and Owen (2007) investigated the irregular particle transport in turbulent flows. Wang and Afsharpoya (2006) used the LBM approach to model the 3-D flow characteristics of a viscous fluid in the serpentine channel of a proton exchange membrane fuel cell (PEMFC). In their approach, the pressure difference between the inlet and the outlet of the PEMFC was modeled using a forcing term such that a periodic boundary condition could still be applied to the density distribution function.

Recent decades have witnessed growing international concern regarding a wide range of environmental issues, including global warming, pollution, the destruction of the rain forests, the accumulation of greenhouse gases, the depletion of non-renewable resources such as oil and gas, and so forth. PEMFCs have emerged as a viable green power source for a range of mobile applications of varying size. Using hydrogen and oxygen as input fuels and producing only water as a byproduct, PEMFCs are widely regarded as an ideal long-term replacement for the gasoline and diesel combustion engines used in today's vehicles. However, to satisfy the requirements for compactness, low cost, high power density, an efficient electrical performance, and stability, it is essential that the design of the PEMFC is fully optimized. Many researchers [Srinivasan, Mankoo, Koch, and Enayetullah (1988), Bernardi and Verbrugge (1992), Wang, Wang, and Chen (2001), Um and Wang (2004)] have used mathematical models to examine the correlation between the PEMFC cell voltage and the current density under various operating conditions. In general, the results have shown that the electrical performance of the fuel cell is dependent upon the velocity characteristics of the reactant gases in the flow channel and gas diffusion layer (GDL). Li (2005), Li and Sabir (2005) reviewed various gas flow channel configurations, including the conventional straight channel, pin-type channels, serpentine channels, interdigitated channels, and so forth. The serpentine flow channel is the most popular design for PEMFC and it can remove the water effectively from the cell. Park and Li (2007) conducted a numerical and experimental investigation into the cross flow through the GDL of a PEMFC with a serpentine flow channel and showed that the total pressure drop between the channel inlet and the channel outlet reduced significantly when the GDL was removed. Hontanon, Escudero, Bautista, Garcia-Ybarra, and Daza (2000) performed computational fluid dynamics (CFD) simulations to investigate the flow field characteristics within gas flow channels with rectangular, trapezoidal, triangular and semi-circular cross-sections.

The present study utilizes a D3Q15 LBM model to simulate the 3-D steady-state flow of a viscous fluid through the serpentine gas flow channel of a PEMFC. The simulations model the velocity distributions within the channel at Reynolds numbers of Re=5, 15 and 25, respectively, and consider three different serpentine channel configurations, namely an empty channel with planar walls, a channel containing a periodic arrangement of 10 rectangular obstacles, and a channel containing a periodic arrangement of 10 semicircular obstacles.

2 Simulation methodology

2.1 Three-dimensional lattice model and equilibrium distribution function

The simulations performed in this study are based on the three-dimensional, fifteen-velocity (D3Q15) LBM model shown in Figure 1. In this model, the lattice streaming speed is given by $c = \delta x/\delta t = \delta y/\delta t$, where δx and δy are the grid spacings in the x- and y-directions, respectively, and correspond to the distances moved by each particle in the x- and y-directions during each time step. The discrete velocities in the D3Q15 model are defined as follows:

$$\begin{bmatrix} \vec{e}_1, & \vec{e}_2, & \vec{e}_3, & \vec{e}_4, & \vec{e}_5, & \vec{e}_6, & \vec{e}_7, & \vec{e}_8, & \vec{e}_9, \\ \vec{e}_{10}, & \vec{e}_{11}, & \vec{e}_{12}, & \vec{e}_{13}, & \vec{e}_{14}, & \vec{e}_{15} \end{bmatrix}$$
$$= \begin{bmatrix} 0 & 1 & 0 & 0 & -1 & 0 & 0 & 1 & -1 \\ 0 & 0 & 1 & 0 & 0 & -1 & 0 & 1 & 1 \\ 0 & 0 & 0 & 1 & 0 & 0 & -1 & 1 & 1 \end{bmatrix}$$
$$\begin{bmatrix} 1 & 1 & -1 & 1 & -1 & -1 \\ -1 & 1 & -1 & -1 & 1 & -1 \\ 1 & -1 & -1 & -1 & -1 & 1 \end{bmatrix} \quad (1)$$

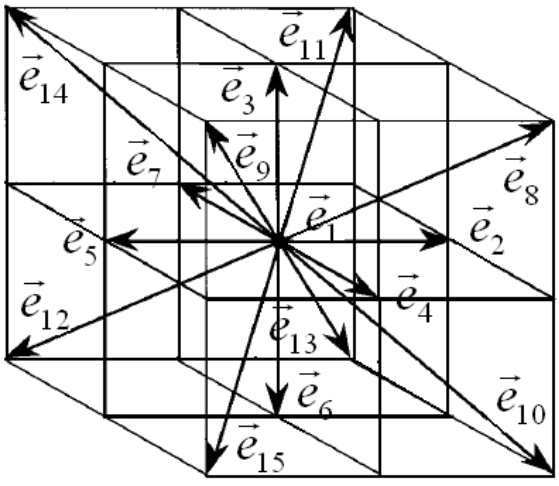

Figure 1: Schematic representation of D3Q15 LBM model.

Of these 15 velocity components, one component has a velocity of 0, six components have a velocity of 1 and eight components have a velocity of $\sqrt{3}$. The evolution of the density distribution function is computed by

$$f_\alpha(\vec{x}+\vec{e}_\alpha\delta t, t+\delta t) - f_\alpha(\vec{x},t) = -\frac{1}{\tau_\upsilon}\left[f_\alpha(\vec{x},t) - f_\alpha^{eq}(\vec{x},t)\right], \quad (2)$$

where τ_υ is the viscosity-based dimensionless relaxation time. Meanwhile, the local equilibrium density distribution is given by

$$f_\alpha^{eq}(\vec{x},t) = \frac{2}{9}\rho\left[1 - \frac{3}{2}\vec{V}^2\right], \quad \alpha = 1 \quad (3)$$

$$f_\alpha^{eq}(\vec{x},t) = \frac{1}{9}\rho\left[1 + 3\left(\vec{e}_i\cdot\vec{V}\right) + \frac{9}{2}\left(\vec{e}_i\cdot\vec{V}\right)^2 - \frac{3}{2}\vec{V}^2\right], \quad \alpha = 2,3,4,5,6,7 \quad (4)$$

$$f_\alpha^{eq}(\vec{x},t) = \frac{1}{72}\rho\left[1 + 3\left(\vec{e}_i\cdot\vec{V}\right) + \frac{9}{2}\left(\vec{e}_i\cdot\vec{V}\right)^2 - \frac{3}{2}\vec{V}^2\right], \quad \alpha = 8,9,10,11,12,13,14,15 \quad (5)$$

In accordance with the kinetic theory of gases, the density ρ and flow velocity $\vec{V}$ within the channel are defined in terms of the density distribution function as follows:

$$\rho = \sum_\alpha f_\alpha, \quad \rho\vec{V} = \sum_\alpha \vec{e}_\alpha f_\alpha. \quad (6)$$

The pressure within the channel is related to the density by $p = c_s^2\rho$, derived from the equation of state for an ideal gas, where $c_s = c/\sqrt{3}$ is the speed of sound. Meanwhile, the kinematic viscosity of the fluid is related to the relaxation time, τ_υ, and the lattice spacing, δx, via

$$\upsilon = \frac{(2\tau_\upsilon - 1)}{6}\delta x. \quad (7)$$

In the current simulations, the density distribution function given in Eq. (2) is solved using a two-step procedure, i.e. a collision step followed by a streaming step. The streaming step requires little computational effort since it simply advances the data from the neighboring lattice points, while the collision step is completely localized.

2.2 Simulation procedure

Figure 2 present a schematic illustration of the serpentine channel considered in the current simulations. As shown, the channel has a width and height of W and an inlet/outlet channel length of 9W. The simulations are performed using a rectangular mesh (201*21*61) and are terminated in accordance with the following convergence criterion:

$$\frac{\sum_{i,j}\left\|\vec{V}(x_{i,j},t+\delta t)-\vec{V}(x_{i,j},t)\right\|}{\sum_{i,j}\left\|\vec{V}(x_{i,j},t)\right\|}\leq 1.0\times 10^{-6}. \tag{8}$$

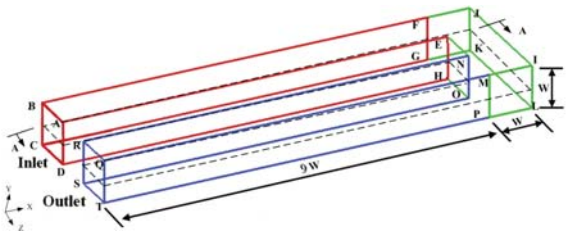

Figure 2: Geometry of conventional 3-D serpentine channel with no obstacles.

The fluid at the inlet ($\overline{ABCD}$) is assumed to have a constant velocity of 0.05. Note that the velocity is specifically assigned a value of less than 10% of the speed of sound in order to avoid generating significant compressibility effects within the fluid. Using the bounce-back rule incorporated in the non-equilibrium distribution function proposed by Zou and He (1997), the equilibrium density distribution function is computed from the pressure and given velocity and is then imposed at the first lattice column within the computational model. At the channel outlet($\overline{QRST}$), a fixed pressure boundary condition is imposed in terms of the equilibrium distribution function, and the velocity components are extrapolated in the upstream direction. The bounce-back rule [Zou and He (1997)] is also used to establish no-slip boundary conditions at the channel walls. The density distribution function at the boundary must satisfy the following condition:

$$f_{\alpha}^{neq}=f_{\beta}^{neq}, \tag{9}$$

where e_{α} and e_{β} act in opposite directions.

As described in the introduction, the current simulations consider three different channel configurations, namely an empty channel with planar wall surfaces, a channel containing rectangular obstacles, and a channel containing semicircular obstacles. In the case of the latter configuration, the non-rectangular boundary is modeled using the second-order accuracy scheme proposed by Guo, Zheng, and Shi (2002).

3 Validation

Prior to the simulations, the validity of the D3Q15 model was evaluated using the 3-D channel configuration shown in Figure 2. In the validation trials, the aspect ratio of the rectangular channel was defined as $AR=a/b$ and the Reynolds number (Re) was given as$Re=U_mD_h/\upsilon$, where U_m denotes the average inlet velocity and D_h the hydraulic diameter, defined as $D_h=2ab/(a+b)$. Finally, the friction factor was defined as

$$f=-\frac{2D_h}{\rho U_m^2}\left(\frac{dp}{ds}\right). \tag{10}$$

It can be shown experimentally that the friction factor for laminar flow is $f=64/Re$ and is valid for engineering calculations involving fluid flows in both smooth and rough circular pipes for values of Re up to approximately 2000. Various analytical methods have been proposed for determining the correlation between the friction factor and the Reynolds number in noncircular ducts. In the current validation trials, the friction factor was derived from the pressure drop along the channel, as evaluated using the D3Q15 LBM model. The product of the friction factor and the Reynolds number ($f\times Re$) was then computed as a function of the aspect ratio. Figure 3 plots the corresponding results for the inlet and outlet sections of the serpentine channel. The results obtained by Olson (1990) are also provided for comparison purposes. The maximum deviation between the present results and those presented in Olson

(1990) occurs at an aspect ratio of$AR = 0.25$ and is found to be less than 1.25 %. Thus, the validity of the current computational model is confirmed.

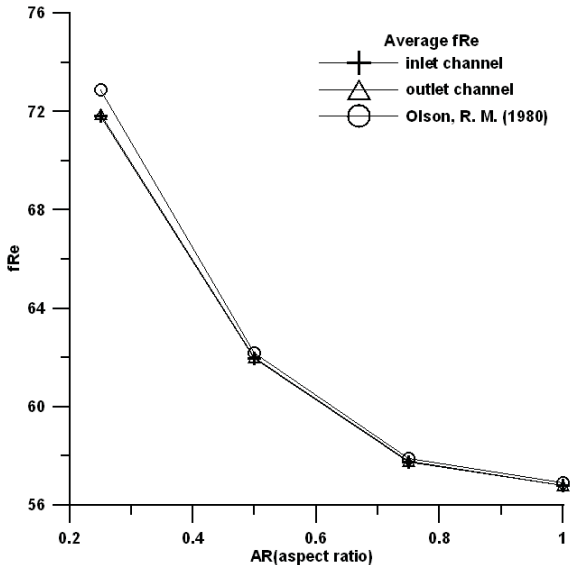

Figure 3: Variation of fRe in inlet and outlet section of channel with aspect ratio. (Note that results presented by Olson R.M. (1980) are also shown for verification purposes.)

4 Results and discussion

4.1 Case I – serpentine channel with no obstacles

Figures 4(a)∼(c) illustrate the velocity distributions at cross-section A-A of the conventional serpentine channel (see Figure 2) in the x-, y- and z-directions, respectively. Note that the Reynolds number is assigned a value of Re=25 in every case. The results show that the maximum velocity in the x-direction occurs in the central region of the inlet channel. However, due to the symmetry of the channel geometry, there is no distribution of the vertical velocity component in the vertical (y) distribution. Finally, the maximum velocity in the z-direction occurs in the U-bend region of the channel as a result of the circuitous effect.

In conventional PEMFCs with straight gas flow channels, the reactant gases are transported through the GDL to the catalyst layer via the effects of diffusion alone. However, diffusion is

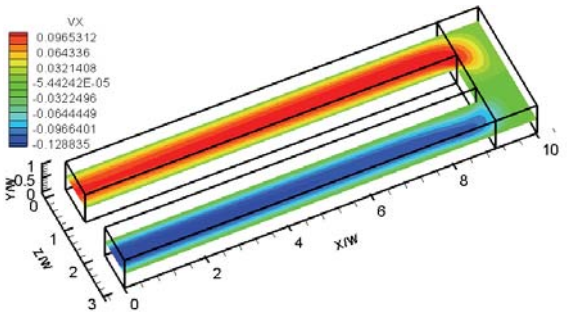

(a) velocity in x direction

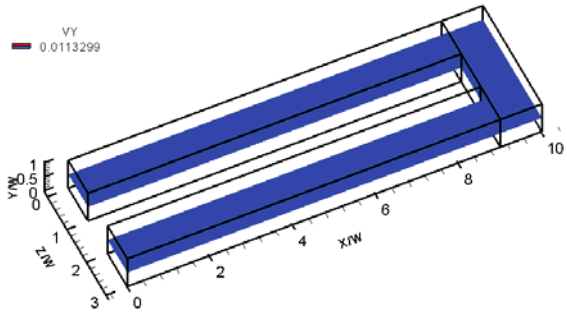

(b) velocity in y direction

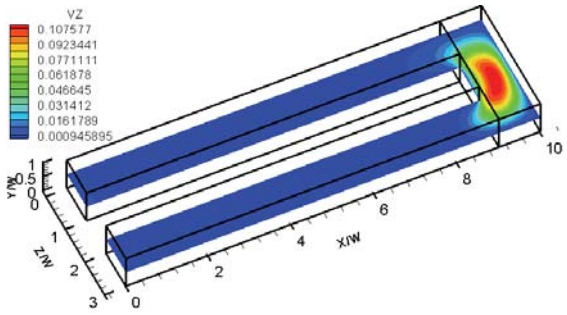

(c) velocity in z direction

Figure 4: Velocity distribution in cross-section A-A of serpentine channel with no obstacles (Re = 25).

an inherently slow process, and hence the performance of the fuel cell is inevitably limited. In practice, the electrical performance of a PEMFC can be improved by increasing the y-direction velocity component of the gas flow such that the rate of transfer of the reactant gas through the GDL is increased. In an attempt to improve the PEMFC performance, the following simulations consider the case where obstacles are introduced within the serpentine channel in order to enhance the velocity of the reactant gas in the vertical direction.

4.2 Case II – serpentine channel with rectangular obstacles

Figure 5 illustrates the case in which 10 rectangular obstacles are placed within the serpentine channel. As shown, each block has a length and width of W and a height of 0.5W. The first block is positioned such that it is located at a distance 1.5W downstream of the inlet. The remaining blocks are arranged such that they are symmetrical to one in the inlet and outlet sections of the channel, respectively, and are separated by a distance of W/2. Figures 6(a)∼(c) present various views of the corresponding streak lines in the inlet section of the channel under a Reynolds number of Re = 25. The streak line chosen for drawing is the one closes the lower wall and due to the inertial force, the fluid behind the square block can not continue the original path to move forward. It results in the separation of boundary layer and the recirculation zone forming behind the block. To prevent the mess of streak line drawing, only the recirculation zone between the first and second obstacle are presented on the Figure 6. It is observed that recirculation zones are formed behind each obstacle. These recirculation structures are a result of the pressure drag effect induced by the acceleration of the main fluid flow stream as it passes through the constricted region of the channel above each of the obstacles. There is also a difference between 2-D and 3-D velocity field phenomenon. In 2-D simulations, it is found that such recirculation structures are closed, i.e. the fluid remains trapped within the recirculation feature and continues to rotate within the local region. However, in the current 3-D simulations, the fluid rotates around the recirculation zone several times and then rejoins the main fluid flow in the upper region of the channel. Figures 7 and 8 illustrate the streak lines in the U-turn region and outlet section of the serpentine channel, respectively. When the fluid passes through the U-turn channel and enters the outlet section, it encounters the first rectangular obstacle almost immediately. As in the inlet channel, the faster velocity in the central region of the channel forces most of the fluid toward the side walls (see Figure 8(a)). Furthermore, recirculation zones are again formed between the obstacles as a result of the pressure drag effect.

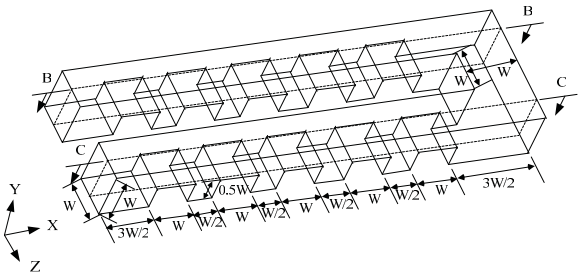

Figure 5: Geometry of serpentine channel containing 10 rectangular obstacles.

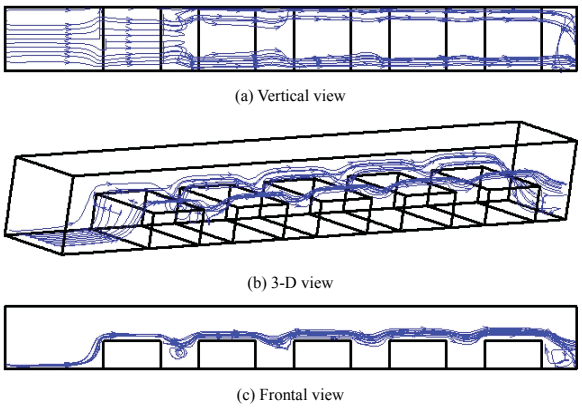

Figure 6: Streak lines in inlet section of serpentine channel containing 5 rectangular obstacles (Re = 25).

Figures 9(a) and 9(b) illustrate the variation of the average y-direction velocity component along the length of the inlet channel and outlet channel, respectively, as a function of the Reynolds number. As shown, the introduction of the rectangular obstacles causes a significant enhancement in the local vertical velocity component. As a result, the rate of transfer of the reactant gas to the GDL is increased, and hence the efficiency of the catalytic reaction is improved. As would be expected, the magnitude of the velocity enhancement increases as the Reynolds number decreases. Note that whilst the obstacles improve the velocity field characteristics of the reactant gases, they also result in a significant pressure loss along the

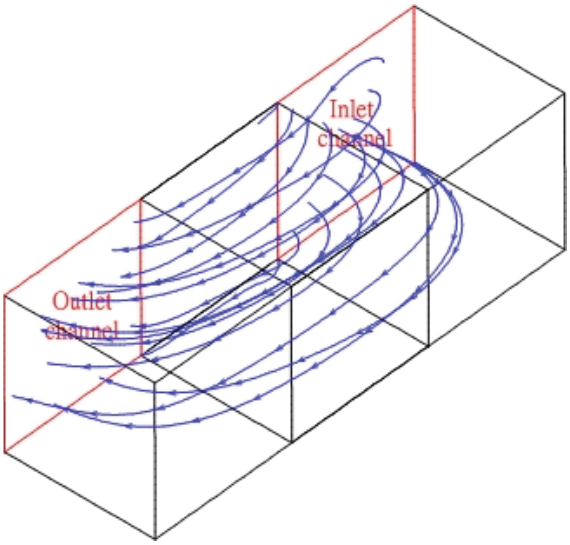

Figure 7: Streak lines in U-turn area of serpentine channel containing 10 rectangular obstacles (Re = 25).

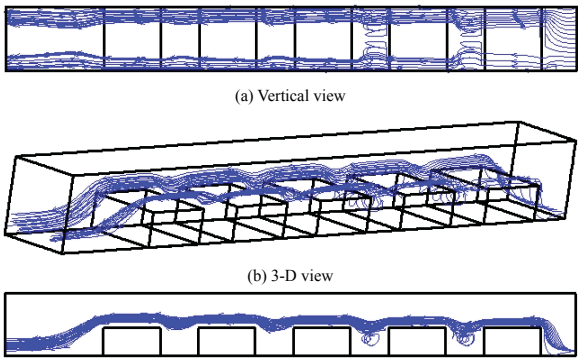

(a) Vertical view

(b) 3-D view

(c) Frontal view

Figure 8: Streak lines in outlet section of serpentine channel containing 5 rectangular obstacles (Re = 25).

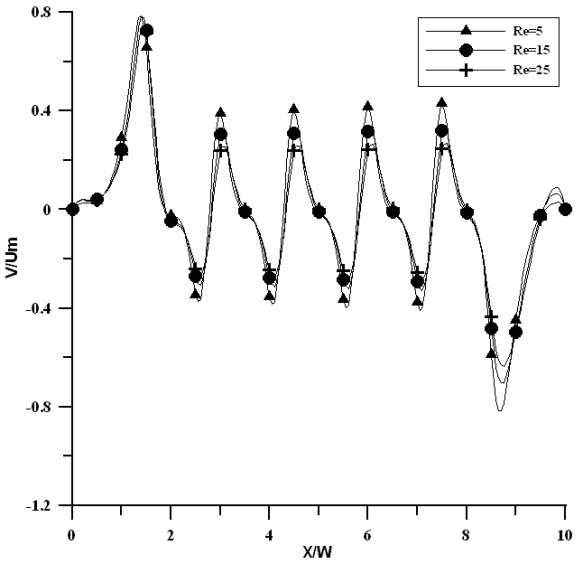

(a) Inlet channel

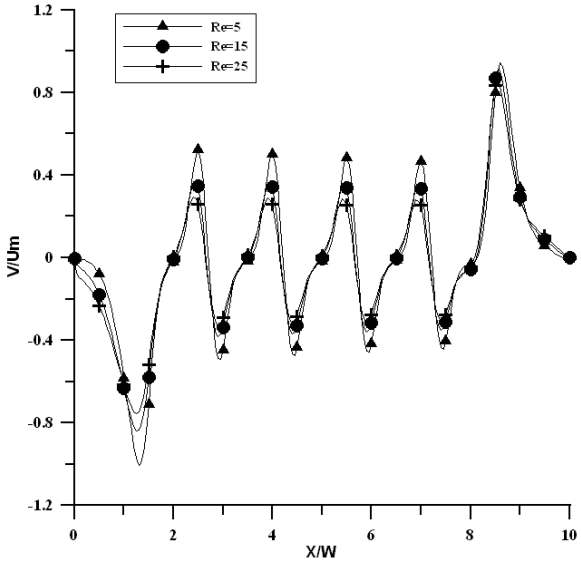

(b) Outlet channel

Figure 9: Variation of average y-direction velocity component in inlet and outlet sections of serpentine channel with 10 rectangular obstacles (Note Re=5, 15 and 25).

channel. Accordingly, a further series of simulations was performed in which the rectangular obstacles were replaced by blocks with a semicircular profile in an attempt to reduce the drag force.

4.3 Case III – serpentine channel with semicircular obstacles

Figure 10 shows the arrangement of the 10 semicircular obstacles within the serpentine channel. As shown, each obstacle has a radius of 0.5W and the first obstacle is located at a distance 1.5W downstream from the inlet. Figures 11 and 12 present the streak lines in the inlet and outlet sections of the channel, respectively, for the case of Re=25. Comparing the streak lines in these figures with those presented in Figures 6 and 8 for

the channel containing rectangular obstacles, it is clear that the lower drag force of the semicircular obstacles allows most of the fluid to flow over the first obstacle relatively unimpeded, i.e. the fluid is pushed toward the side walls of the channel only at the second obstacle and beyond. The recirculation zone generating in the square block channel is also appearing in circle shape type. As in the channel containing rectangular blocks, Figures 11 and 12 reveal that the semicircular obstacles induce a pressure drag effect, which results in the formation of open recirculation structures between neighboring obstacles.

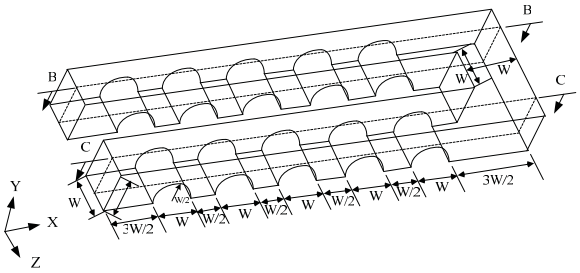

Figure 10: Geometry of serpentine channel containing 10 semicircular obstacles.

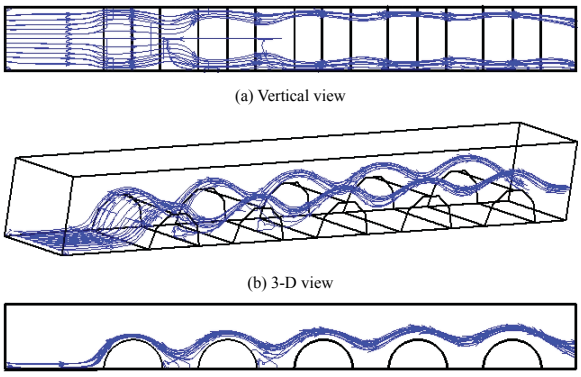

Figure 11: Streak lines in inlet section of serpentine channel containing 5 semicircular obstacles (Re = 25).

Figure 13 shows the influence of Reynolds number on average y-direction velocity component along the height of 0.75 W serpentine channel with 10 semicircle block obstacles. Figures 13(a)

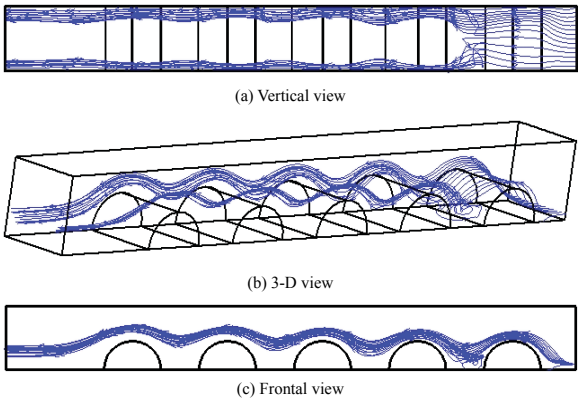

Figure 12: Streak lines in outlet section of serpentine channel containing 5 semicircular obstacles (Re = 25).

and 13(b) present the variation of the average y-direction velocity component along the inlet and outlet sections of the channel, respectively, as a function of the Reynolds number. It can be seen that the semicircular obstacles yield a significant increase in the local vertical velocity component and are therefore beneficial in improving the catalytic performance of the fuel cell. Furthermore, comparing Figure 13 with Figure 9, it is apparent that the semicircular obstacles induce a smoother variation in the vertical flow velocity than the rectangular obstacles as a result of their lower drag force.

Finally the friction factor is discussed here. In order to increase the velocity in y-direction and therefore increase the obstacles in the channel. The following side effect needs to be considered. The friction drag force imposed on the reactant gases by the obstacles within the serpentine channel can be quantified via the product $f \times Re$. Figures 14(a) and 14(b) illustrate the variation of $f \times Re$ along the inlet and outlet sections of the three serpentine channels considered in the current simulations. From inspection, the average value of $f \times Re$ over the entire length of the empty serpentine channel is found to be 56.81, while that of the channels with rectangular and semicircular obstacles is found to be 236.42 and 164.05, respectively. In other words the rectangular and semicircular obstacles increase the drag force by around 3.16 and 1.89 times. Then, the augmen-

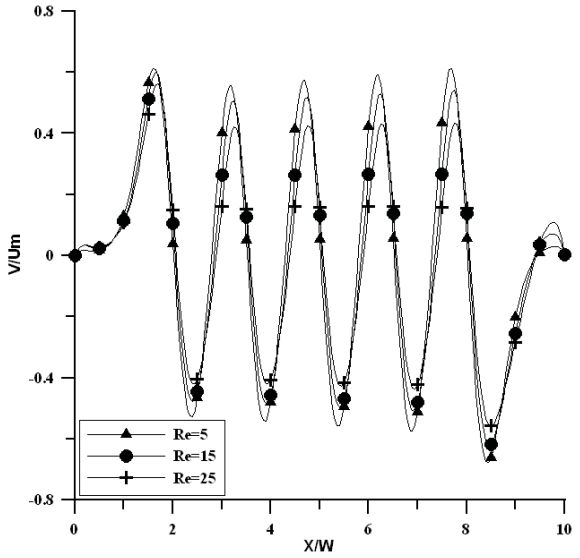

(a) Inlet channel

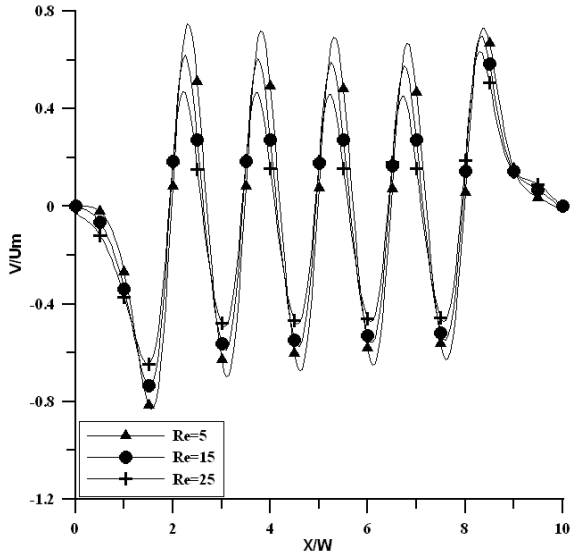

(b) Outlet channel

Figure 13: Variation of average y-direction velocity component in inlet and outlet sections of serpentine channel with 10 semicircular obstacles (Note Re=5, 15 and 25).

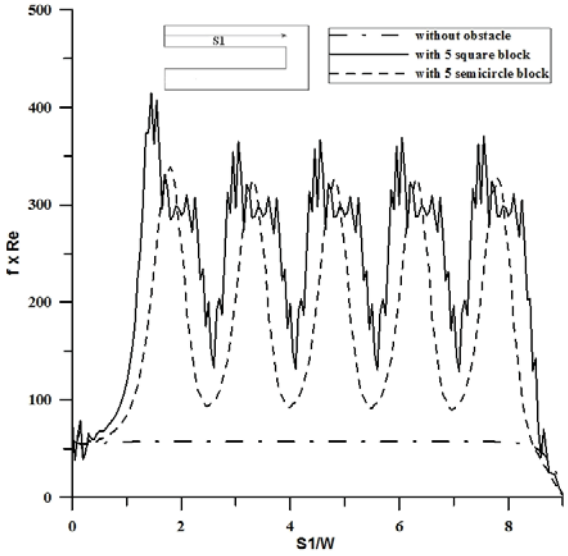

(a) Inlet channel

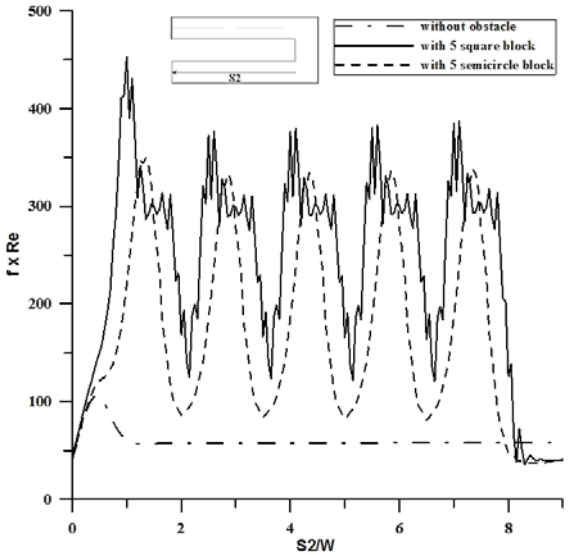

(b) Outlet channel

Figure 14: Variation of drag force along inlet and outlet sections of three serpentine channel configurations (Re=25).

tation of the dispersion due to obstacles would be assessed versus the product $f \times Re$. We defined the V'/S_1 and V'/S_2 as y-direction flow rate per length in the inlet and outlet channel. Although the channel without the obstacles produces the lowest friction drag force, it also creates the lowest y-direction flow rate. Tables 1 (Re=25) indicate that while we set the obstacles will increase the drag force, but it will augment y-direction flow rate. Clearly, the lower drag forces of the semicircular obstacles result the more y-direction flow rate. It renders them a more appropriate choice for improving the catalytic performance of the PEMFC than the rectangular blocks.

Table 1: Y-direction flow rate versus the friction drag force at Re=25

Inlet channel	**5 blocks**	**5 waves**	**No obstacles**
V'/S_1	0.0912026	0.1242584	0.0000458
$f \times \mathrm{Re}$	233.4940110	162.8023922	56.8022903
$(V'/S_1)\,/\,(f \times \mathrm{Re})$	0.0003906	0.0007632	0.0000008
Outlet channel	**5 blocks**	**5 waves**	**No obstacles**
$V'S_2$	0.0966133	0.1309626	0.0000059
$f \times \mathrm{Re}$	239.3636064	165.2958513	56.8105594
$(V'/S_2)\,/\,(f \times \mathrm{Re})$	0.0004036	0.0007923	0.0000001

5 Conclusions

In this study, the LBM was applied to simulate 3-D incompressible steady flow under low Reynolds number in serpentine channel and analyze the local influence on flow field caused by inserting two types of obstacles (square block and semicircle block). The most concern in this paper is using the new computation tool LBM to solve 3-D flow field. Using the D3Q15 LBM model, this study has performed a series of LBM simulations to investigate the 3-D velocity field characteristics of a viscous fluid flowing along the serpentine channel of a PEMFC at Reynolds number ranging from Re=5$\sim$25. The simulations have considered three specific serpentine channel configurations, namely a conventional channel with planar upper and lower walls, a channel containing a periodic arrangement of rectangular obstacles and a channel containing a periodic arrangement of semicircular obstacles. In general, the results have shown that the obstacles induce a local enhancement of the vertical velocity component of the gas flow. This improves the performance of the PEMFC since it increases the supply of the reactant gases to the catalyst layers and therefore improves the efficiency of the catalytic reaction. It has been shown that the obstacles induce the formation of recirculation structures within the fluid flow as a result of a pressure drag effect. These recirculations are open-type structures and therefore assist in the removal of water vapor from the cathode side of the PEMFC, thereby reducing the membrane drowning effect. While both types of obstacle increase the friction drag acting on the fluid within the channel, the semicircular obstacles generate a lower drag force and more flow rate. Therefore, semicircular obstacles represent a more appropriate choice for enhancing the gas flow rate through the GDL. On one hand, this study verifies the capability of the method to solve the fluid with complex geometry. On the other hand, this study gives the first step for further exploration of PEMFC's problem.

References

Nicolas, A.; Bermudez, B. (2004): 2D Incompressible Viscous Flows at Moderate and High Reynolds Numbers. *CMES: Computer Modeling in Engineering & Sciences*, vol. 6, no. 5, pp. 441-451.

Chen, S.; Doolen, G.D. (1998): Lattice Boltzmann method for fluid flows. *Annu. Rev. Fluid Mech.*, vol. 30, pp. 329-364.

He, X.; Chen, S.; Doolen, G.D. (1998): A novel thermal model for the Lattice Boltzmann method in incompressible limit. *Journal of Computational Physics*, vol. 146, pp. 282-300.

Wolf-Gladrow, D.A. (2000): *Lattice gas cellular automata and Lattice Boltzmann models: An introduction*. Springer-Verlag Berlin.

Succi, S. (2001): *The Lattice Boltzmann method for fluid dynamics and beyond*. Oxford Univ. Press Oxford England U. K..

Chen, C.K.; Chang, S.C.; Sun, S.Y. (2007): Lattice Boltzmann Method Simulation of Channel Flow with Square Pillars inside by the Field Synergy Principle. *CMES: Computer Modeling in Engineering & Sciences*, vol. 22, no. 3, pp. 203-215.

Qian, Y.H.; d'Humieres, D.; Lallemand, P. (1992): Lattice BGK models for Navior-Stokes

equation. *Europhy. Lett.*, vol. 17, pp. 479-484.

Han, K.; Feng, Y.T.; Owen, D.R.J. (2007): Numerical Simulations of Irregular Particle Transport in Turbulent Flows Using Coupled LBM-DEM. *CMES: Computer Modeling in Engineering & Sciences*, vol. 18, no. 2, pp. 87-100.

Wang, L.P.; Afsharpoya, B. (2006): Modeling fluid flow in fuel cells using lattice-Boltzmann approach. *Mathematics and Computers in Simulation,* vol. 72, pp. 242-248.

Srinivasan, S.; Mankoo, D.J.; Koch, H.; Enayetullah, M.A. (1988): Recent advances in solid polymer electrolyte fuel cell technology with low platinum loading electrodes. *Journal of Power Sources*, vol. 29, pp. 367-387.

Bernardi, D.M.; Verbrugge M.W. (1992): A mathematical model of the solid-polymer-electrolyte fuel cell. *Journal of The Electrochemical Society*, vol. 139, pp. 2477-2491.

Wang, Z.H.; Wang, C.Y.; Chen, K.S. (2001): Two-phase flow and transport in the air cathode of proton exchange membrane fuel cells. *Journal of Power Sources*, vol. 94, pp. 40-50.

Um, S.; Wang, C.Y. (2004): Three-dimensional analysis of transport and electrochemical reactions in polymer electrolyte fuel cells. *Journal of Power Sources*, vol. 125, pp. 40-51.

Li, X. (2005): *Principles of Fuel Cells*. Taylor & Francis, New York.

Li, X.; Sabir, I. (2005): Review of bipolar plates in PEM fuel cells: Flow-field designs. *Int. J. Hydrogen Energy*, vol. 30, pp. 359-371.

Park, J.; Li X. (2007): An experimental and numerical investigation on the cross flow through gas diffusion layer in a PEM fuel cell with a serpentine flow channel. *Journal of Power Sources*, vol. 163, pp. 853-863.

Hontanon, E.; Escudero, M.J.; Bautista, C.; Garcia-Ybarra, P.L.; Daza, L. (2000): Optimization of flow-field in polymer electrolyte membrane fuel cells using computational fluid dynamics technique. *Journal of Power Sources*, vol. 86, pp. 363-368.

Zou, Q.; He, X. (1997): On pressure and velocity boundary conditions for the lattice Boltzmann BGK model. *Phys. Fluids*, vol. 9, pp. 1591-1598.

Guo, Z.; Zheng, C.; Shi, B. (2002): An extrapolation method for boundary conditions in lattice Boltzmann method. *Physics of fluids*, vol. 14, pp. 2007-2010.

Olson, R.M. (1990): *Essentials of engineering fluid mechanics*, Harper & Row, New York.